AFOSR GRANT:	Dynamics of $O(^3P)$ Reactions with Gaseous, Liquid, and Solid Hydrocarbons
AFOSR PROGRAM MANAGER:	Michael Berman
CONTRACT NUMBER:	FA9550-04-1-0373
PRINCIPAL INVESTIGATOR (PI):	William L. Hase
PI INSTITUTION:	Texas Tech University
PI ADDRESS:	Department of Chemistry and Biochemistry Lubbock, Texas 79409-1061

Objectives: to model and simulate the chemical dynamics of $O(^3P)$ reaction with hydrocarbon monomers, small clusters, liquids, solids, and self-assembled monolayer (SAM) surfaces.

Accomplishments:

- Ab initio calculations on model reactions to generate a database of accurate energies and geometries.[1]
- Least squares fit of semiempirical PM3 theory to the ab initio database. The reparametrized potential is called PM3-SRP (PM3 with specific reaction parameters).
- Use of PM3-SRP in quasiclassical trajectory calculations of the dynamics of $O(^3P)$ reactions with hydrocarbons.

  Applications:

  - $O(^3P)$ + ethane at 5 eV collision energy.[2]
  - $O(^3P)$ + propane monomer and tetramer at < 2 eV collision energy (manuscript in preparation).[3]
  - Energy transfer and physisorption of $O(^3P)$ on alkane monolayer surfaces (manuscript accepted).[4]

Introduction. Reactions of the electronically ground-state oxygen atom $O(^3P)$ with hydrocarbons are of considerable interest because of their importance in combustion and atmospheric chemistry,[5,6,7] and in processing hydrocarbon surfaces.[8] Extensive gas-phase studies of $O(^3P)$ reaction with alkanes (RH) at low collision energies, where the only reactive channel is have provided detailed information of product internal state distributions,[6,7] scattering angles of

$$O(^3P) + RH \rightarrow OH\cdot + R\cdot$$

the reaction products,[7] and rate constants.[9] For the $O(^3P) + CH_4$ and $O(^3P) + C_2H_6$ reactions studied here, the recommended expressions for the thermal rate constants are, respectively, $(1.15 \times 10^{-15}) T^{1.56} \exp(-4270/T)$ $cm^3 molecule^{-1} s^{-1}$ for T = 300-2500 K[10] and $(1.8 \times 10^{-31}) T^{6.5} \exp(-140/T)$ $cm^3 molecule^{-1} s^{-1}$ for T = 298-1300 K.[11] Some uncertainties remain in the temperature-dependent rate constants as illustrated by the alternative expression $(2.69 \times 10^{-18}) T^{2.3} \exp(-3570/T)$ $cm^3 molecule^{-1} s^{-1}$ suggested[12] for $O(^3P) + CH_4$.

$O(^3P)$ is used in chemical processing of hydrocarbon surfaces to make polymeric materials for technological and industrial applications.[13] Chemical processing by $O(^3P)$ atoms may also be detrimental by damaging polymeric coatings. This is particularly problematic for spacecraft in a low Earth orbit (LEO).[14] Spacecraft in LEO travel at a velocity of approximately 8 km/s, giving rise to a relative translational energy of ~5 eV for an O-atom striking the spacecraft. Under such harsh conditions there is considerable erosion of the spacecraft's surface. Recently, several experimental[8,15,16] and computational studies[17,18,19] have been performed to probe the kinetics and mechanisms for $O(^3P)$ reactions with hydrocarbon surfaces.

At high collision energies other reaction channels, in addition to reaction (1), are open for the $O(^3P)$ atom. From *ab initio* calculations, Massa and coworkers[20] identified a C-C bond rupture channel, which for ethane forms CH_3 and OCH_3. Schatz and coworkers[18,19] extended these calculations and also identified a C-H bond rupture channel; i.e. $O(^3P) + RH \longrightarrow H + OR$. For the $O(^3P) + C_2H_6$ system the threshold energy is approximately 2 eV for both the C-C and C-H bond rupture channels.[19] For high collision energies, such as 5 eV in LEO, it is expected that a large amount of energy will be deposited in the internal modes of the ethoxy radicals by the C-C and C-H bond rupture channels, leading to unimolecular dissociation of the species. Schatz and coworkers[19,21] have performed direct dynamics simulations with the MSINDO semiempirical

theory to study the primary reaction channels for $O(^3P) + C_2H_6$ collisions at 3.26 eV to compare with the experimental study[21] of Minton and coworkers. In this report we describe a similar direct dynamics simulation at 5 eV using a PM3-SRP semiempirical model, in which the trajectories are integrated for a sufficiently long time to investigate the dissociation of the alkoxy radicals formed by the primary reaction channels.

Multi-reference ab initio calculations.[1] Electronic structure calculations based on multi-configuration wave functions were used to investigate the energetics, transition states, and intrinsic reaction coordinates of a set of prototypical reactions for $O(^3P)$ processing of hydrocarbon molecules and surfaces. The specific reactions studied are

$$O(^3P) + CH_4 \longrightarrow OH + CH_3 \quad \text{(R1)}$$

$$O(^3P) + C_2H_6 \longrightarrow OH + C_2H_5 \quad \text{(R2)}$$

$$OH + C_2H_6 \longrightarrow H_2O + C_2H_5 \quad \text{(R3)}$$

$$OH + C_2H_5 \longrightarrow H_2O + C_2H_4 \quad \text{(R4)}$$

$$OH + C_2H_5 \longrightarrow H_2O + CH_3CH \quad \text{(R5)}$$

$$O(^3P) + C_2H_6 \longrightarrow CH_3O + CH_3 \quad \text{(R6)}$$

$$O(^3P) + C_2H_6 \longrightarrow C_2H_5O + H \quad \text{(R7)}$$

For all reactions except R4, only the lowest triplet state is examined. Singlet spin states are not considered. Reactions R4-R6 are possible secondary reactions derived from R2. Reaction R5 gives triplet ethylene, $^3C_2H_4$, which is twisted 90°, and R6 gives triplet methylcarbene, $^3CH_3CH$.

Reactions R1-R6 were examined with CASSCF,[22] second and third order Rayleigh-Schrödinger perturbation theory with a CASSCF reference (CASPT2,[23,24] CASPT3[23]), and internally contracted multi-reference configuration interaction (MRCI).[25] The calculations were

performed using MOLPRO 2002.3[26] for ROHF, CASSCF, CASPT2/3, and MRCI, and GAMESS 98[27] for the IRC calculations with CASSCF. At CASSCF and CASPT2 optimized geometries, single point energy corrections are computed with MRCI+Q (MRCI with the Davidson correction for quadruple excitations) and the cc-pVTZ and cc-pVQZ basis sets, with extrapolation to the complete basis set limit (designated CBL) using two-point power law extrapolation.[28] For R1-R6, the active spaces were (10,10), (8,8), (4,4), (9,9), (10,10), (8,8), respectively. Geometry optimization and frequency calculations were carried out with CASSCF/cc-pVTZ for all reactions, and also with CASPT2/cc-pVTZ for R1-R3.

Table 1. CASPT2/CBL and MRCI+Q/CBL values of barriers and energies of reaction at 0 K for reactions R1-R6.[a]

	Barrier at 0 K			Energy of reaction at 0 K		
	CASPT2	MRCI+Q	best estimate	CASPT2	MRCI+Q	expt[b]
R1	7.9	10.5	10 ± 1[c]	-0.1	1.4	1.6 ± 0.2
R2	5.3	9.0	7 ± 1[d]	-4.6	-1.4	-5.5 ± 1.4
R3	41.3	46.9	—	2.9	1.1	-1.9 ± 10
R4	0.6	2.8	1 - 2[e]	-18.8	-17.4	-21.3 ± 1.4
R5	1.4	3.2	—	-19.0	-17.8	-22.7 ± 4
R6	2.0	3.8	—	-10.7	-10.8	-14.4 ± 5

[a]Stationary points optimized with CASPT2/cc-pVTZ for reactions 1 and 2, CASSCF/cc-pVTZ for others.

[b]http://srdata.nist.gov/cccbdb, IV.A.1. Experimental enthalpies at 0 K.

[c]O. Roberto-Neto, F. B. C. Machado, and D. G. Truhlar, *J. Chem. Phys.* **111**, 10046 (1999).

[d]Reference 1.

[e]Classical barrier from Y.-Y. Chuang, E. L. Coitino, and D. G. Truhlar, *J. Phys. Chem. A* **104**, 446 (2000); ZPE taken from CASSCF(9,9)/cc-pVTZ frequencies.

Table 1 summarizes the CASPT2/CBL and MRCI+Q/CBL 0 K barriers and energies of reaction. The best agreement (within experimental error) is found for MRCI+Q/CBL applied to R1, the only reaction for which the active space preserves the full symmetry of reactants, transition state, and products, while still including all orbitals that undergo significant bonding

changes. The MRCI+Q/CBL 0 K energies of reaction for R2-R6 are more endothermic than experiment by 3-5 kcal/mol. A likely reason for the discrepancies is that, except for R1 and R3, the CASSCF active spaces do not treat the C-H bonds uniformly for reactants, TS, and products. Another source of error in R4-R6 is that MRCI was not able to accommodate reference spaces that include all the bonds that undergo significant changes during the reactions.

Modification of PM3 integrals and PM3-SRP parametrization. The potential V used for trajectories is defined by

$$V = V_{PM3-SRP} + V_{analytical} \tag{1}$$

where $V_{PM3\text{-}SRP}$ is the PM3 semiempirical potential as implemented in the Mopac 7 package,[29] modified as described below, and $V_{analytical}$ describes long range O-H and O-C interactions. $V_{analytical}$ is given by

$$V_{analytical} = \sum_{i = O-C,\, O-H} \frac{1}{2}\left[1 + \tanh\left(f_i(r_i - r_{i0})\right)\right]\left[a_i \exp(-b_i r_i) + c_i r_i^{-6}\right], \tag{2}$$

where i refers to O-H or O-C interactions, r_i is the distance, and $V_{analytical}$ is characterized by the 10 parameters f_i, r_{i0}, a_i, b_i, c_i (Appendix, Table A1). $V_{PM3\text{-}SRP}$ is constructed with 65 parameters. 29 of these are conventional PM3 parameters for C, O, H listed in Table A2. The remaining 36 parameters (Tables A3, A4) are associated with modified resonance integrals (two-center one-electron integrals) H_{ij}^{ab} given by

$$H_{ij}^{ab} = \chi_{ij}^{ab}(r_{ij}) H_{ij}^{0,ab}, \tag{3}$$

where $\chi_{ij}^{ab}(r_{ij})$ is a distance-dependent multiplier and $H_{ij}^{0,ab}$ is the original PM3 resonance integral between atoms *i* and *j*, *ab* labels the overlap type (*ss, sp, pp*), and r_{ij} is the *i-j* distance. The multiplier is defined by

$$\chi_{ij}^{ab}(r_{ij}) = \chi_{ij,small}^{ab} + \frac{1}{2}\left(\chi_{ij,large}^{ab} - \chi_{ij,small}^{ab}\right)\left[1 + \tanh\left(f_{ij}\left(r_{ij} - r_{ij}^{0}\right)\right)\right], \qquad (4)$$

which switches from $\chi^{ab}_{ij,small}$ at small values of r_{ij} to $\chi^{ab}_{ij,large}$ at large distance. O-H interactions were treated differently for H-abstraction by O(^{3}P) to form OH (OH_1 column in Tables A3, A4) and abstraction by OH to form H_2O (OH_2 column). This greatly improved the fit to barriers and enthalpies of reaction for the two reaction types. Each trajectory was started with OH_1 parameters, and these were switched to OH_2 parameters only in the rare event that the initially formed OH abstrated a second H-atom. The switch from OH_1 to OH_2 parameters was implemented when the following distance criteria were met: O-H < 1.2 Å, C-H > 1.5 Å, and O-C > 2.7 Å. Although the switch is discontinuous, in practice the tanh switching functions prevented sudden jumps in energy and gradient during the switch.

The 65 parameters of $V_{PM3\text{-}SRP}$ plus 10 parameters for $V_{analytical}$ were determinied by minimizing the weighted sum of squared differences between *V* and best estimates (ab initio or experiment) for barriers, energies of reaction, and geometries of stationary points. The fitting involves minimizing the sum of squares

$$w_E^2\sum_i\left(E_i - E_i^0\right)^2 + w_R^2\sum_i\left(R_i - R_i^0\right)^2 + w_A^2\sum_i\left(A_i - A_i^0\right)^2 + w_D^2\sum_i\left(D_i - D_i^0\right)^2 + w_C^2\sum_i\left(C_i - C_i^0\right)^2$$

where the difference terms involve PM3-SRP minus ab initio energies, bond lengths, bond angles, dihedral angles, and Mulliken atomic charges, and w are weighting factors. The *Fortran*

GA genetic algorithm program of D. A. Carroll was used. The ab initio database consisted of 78 data points: 26 energies, 20 bond lengths, 18 bond angles, 10 dihedral angles, and 4 atomic charges.

The integral definitions described above have been used in high energy $O(^3P)$ + ethane trajectories[2] and low energy trajectories of $O(^3P)$ + propane monomer and tetramer.[3]

$O(^3P)$ + ethane trajectories at 5 eV collision energy. Full details have been published,[2] and a summary is given here. Two parametrization models were examined. In Model 1, the ab initio database was based on reactions R2-R6. This is appropriate for low collision energies at which H-abstraction is the only accessible reaction. To examine higher energy collisions, single reference ab initio calculations were performed at the PMP2/cc-pVTZ//UMP2/cc-pVTZ level of theory. A second parametrization, Model 2, was carried out in which the database included a variety of reactions with high barriers accessible at 5 eV. Table 2 gives a comparison of PM3-SRP Model 2 with the ab initio data.

To calculate the classical trajectories, Hamilton's equations of motion are integrated with a combined 4th-order Runge-Kutta and 6th-order Adams-Moulton predictor-corrector algorithm.[30] This was carried out in VENUS-MOPAC,[31] a combination of VENUS[32] and MOPAC,[29] which PM3-SRP is incorporated and called whenever energies and derivatives are needed. There are two criteria for terminating a trajectory: (1) non-reactive trajectories are terminated when the center-of-mass separation between $O(^3P)$ and C_2H_6 is larger than 7 Å after the collision's inner turning point in the $O(^3P)$ and C_2H_6 relative motion; (2) reactive trajectories are integrated up to 500 fs to monitor possible secondary reactions.

Table 2. PM3-SRP Model 2 *vs ab initio* energies (kcal/mol).[a]

	Reaction	PM3-SRP Model 2		ab initio	
		$\Delta E^{\ddagger}$	ΔE^0	$\Delta E^{\ddagger}$	ΔE^0
P1[b]	$O(^3P) + C_2H_6 \rightarrow OH + C_2H_5$	9.0	-16.0	9.0	-1.4
P2	$O(^3P) + C_2H_6 \rightarrow H + C_2H_5O$	34.5	9.2	48.3	11.8
P3	$O(^3P) + C_2H_6 \rightarrow$ □□$_3$ + CH_3O	51.3	-5.7	46.9	1.1
S1	$OH + C_2H_5 \rightarrow H_2O + {}^3C_2H_4$	8.9	-17.3	4.3	-17.8
S2	$OH + C_2H_5 \rightarrow H_2O + {}^3CH_3CH$	7.9	-10.4	4.9	-10.2
S3	$H + C_2H_5O \rightarrow CH_2CH_2O + H_2$	0.1	-3.7	14.5	1.2
S4	$H + C_2H_5O \rightarrow CH_2CH_2O + H_2$	-1.5	-8.3	9.6	-6.0
S5	□□$_3$ + $CH_3O \rightarrow$ □□$_2$□□□$_□$	6.8	-12.0	13.3	-9.2
UD1	$C_2H_5O \rightarrow CH_3 + CH_2O$	16.5	0.1	14.4	5.3
UD2	$C_2H_5O \rightarrow H + CH_3CHO$	9.1	14.2	24.7	6.4
UD3	$CH_2CH_2O \rightarrow CH_2 + CH_2O$	15.1	11.3	21.8	12.4
UD4	$CH_3CHO \rightarrow CH_3 + CHO$	22.3	6.5	9.8	-3.7
UD5	$CH_3O \rightarrow H + CH_2O$	8.5	15.0	20.4	11.9
UD6	$CH_2O \rightarrow H + CHO$	14.2	20.6	14.1	3.4

[a]ZPE corrected (0 K energies).
[b]P1, P3, S1, and S2 are calculated with MRCI+Q/CBL, all others with PMP2/vtz//UMP2/vtz.

Table 3 gives cross sections for the reactive channels computed from over 50000 trajectories. A substantial amount of the 5 eV collision energy is deposited into the CH_3O and C_2H_5O products of channels 3 and 2 and, as a result, these primary products undergo secondary unimolecular reactions. This leads to a large number of reaction products and small cross sections for channels 2 and 3. Since channel 1 occurs by a stripping mechanism, only a small fraction of the 5 eV collision energy is deposited in the C_2H_5 product. Little dissociation of C_2H_5 to $H + C_2H_4$ occurs, as shown by the large cross section for channel 1 and the much smaller cross section for channel 4. Because of the importance of unimolecular dissociation for the products of primary channels 2 and 3, the cross sections calculated from the trajectories strongly depends on the length of time the trajectories are integrated. Fewer product channels would have been

Table 3. Reaction cross sections of different channels.

Channel	Products[a]	Apparent reaction path[b]	Cross section, Å^2	
			Model 1	Model 2
1	$OH + C_2H_5$	P1	7.14	7.76
2	$C_2H_5O + H$	P2	0.30	0.009
3	$CH_3O + CH_3$	P3	0.025	0.014
4	$OH + C_2H_4 + H$	P1 → UD7	0.082	0.046
5	$H_2O + {}^3C_2H_4$	P1 → S1	0.031	0.019
6	$H_2O + CH_3CH$	P1 → S2	0.31	0.14
7	$CH_3CHO + 2H$	P2 → UD2	2.06	1.17
8	Ethylene oxide + 2H	P2 → UD2 → isom[c]	0.13	0.057
9	$CH_2CH_2O + H_2$	P2 → S3	0.021	< 0.001
10	$^3CH_3CHO + H_2$	P2 → S4	0.087	< 0.001
11	$CH_2O + CH_3 + H$	P2 → UD1 P3 → UD5	0.80	0.65
12	$CH_2O + CH_2 + H_2$	P2 → S3 → UD3	0.026	0.042
13	$CHO + CH_3 + H_2$	P2 → S4 → UD4	0.77	0.41
14	$CHO + CH_4 + H$	P3 → S5 → UD6	0.27	0.071
15	$CH_2CHO + H_2 + H$			0.20
16	$CH_2{=}C{=}O + H_2 + 2H$		0.060	0.072
17	$C_2H_2O + 2H_2$		0.17	0.007
18	$CO + CH_3 + H_2 + H$		0.14	0.93
19	$CO + CH_2 + 2H_2$			0.084
20	$CO + CH_4 + 2H$			0.016
21	$CH_3CHOH + H$	P2 → isom		0.061
22	$^3CH_2{=}CHOH + H_2$	P2 → S3 → isom		0.014

[a]Ground state triplet potential energy surface.
[b]Nomenclature for reaction paths is defined in Table 2.
[c]Isom means the product isomerizes.

observed if the trajectories were only integrated for 100 ps instead of the 500 ps calculated here. Indeed, the trajectory cross sections may change and additional products formed if the trajectories were integrated for an even longer time. Some of the products observed at 500 ps may have sufficient energy to unimolecularly dissociate on a longer timescale.

$O(^3P)$ Reactions with Propane Monomer and Tetramer at < 2 eV Collision Energy.[3]

At low collision energy, H-abstraction is the only open channel for $O(^3P)$ + propane, leading to

$$O(^3P) + CH_3CH_2CH_3 \rightleftharpoons \begin{matrix} OH + CH_3CH_2CH_2 \\ OH + CH_3CHCH_3 \end{matrix}$$

$$OH + CH_3CH_2CH_2 \rightleftharpoons \begin{matrix} H_2O + CH_3CH_2\ddot{C}H \\ H_2O + CH_3\dot{C}HCH_2\cdot \end{matrix}$$

OH + *n*-propyl and isopropyl radicals. Subsequent reaction of OH + propyl on the triplet potential energy surface can give H_2O plus two products, triplet propylene and a triplet carbene. In our initial parametrization (parameter set L1, where L refers to low collision energy), the energies in the database included best estimate barriers and experimental 0 K reaction energies in Table 1. As discussed below, this gave a hotter product OH rotational distribution than experiment.[33] In our current parameter set, L2, the database was augmented with calculations of the O-H-C bending potential for $O(^3P) + C_2H_6 \rightarrow OH + C_2H_5$, using the BB1K density functional,[34] which is optimized to reproduce barriers. Figure 1 compares the O-H-C bending potential of BB1K/6-31G* and PM3-SRP with the L1 and L2 parameter sets. The L2 curve is very close to BB1K at $\leq$ 15 kcal/mol above the saddle point (minimum of the curve), and is reasonably close at higher energies also. Table 4 shows the PM3-SRP L1 and L2 fits to reactions 2-6 used in the parametrization, as well as the $O(^3P) + C_3H_8$ reactions shown above. Barriers and reaction energies are in reasonable agreement with experiment, where available.

Parameter sets L1 and L2 are given in the Appendix. Table A1 gives the parameters for $V_{analytical}$, eq 2; Table A2 lists conventional PM3 parameters accessible through the MOPAC keyword 'EXTERNAL'; Tables A3 and A4 give the parameters associated with the distance-dependent integral multipliers, eq 3 and 4.

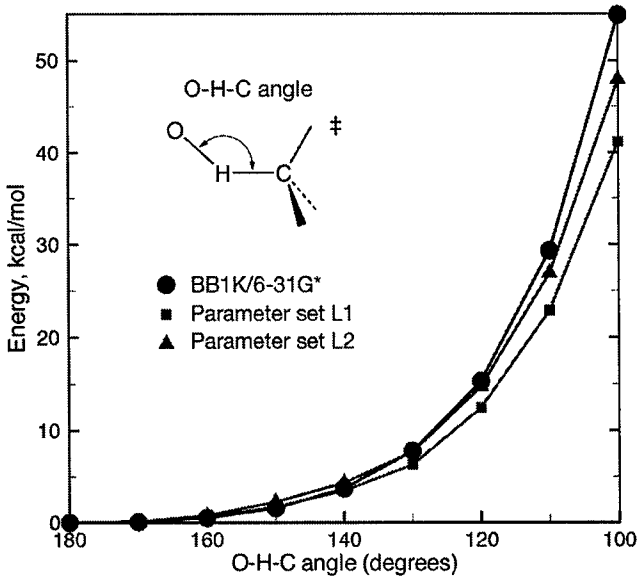

Figure 1. Energy vs O-H-C bending angle in the transition state for H-abstraction from ethane by $O(^3P)$, for BB1K/6-31G* and PM3-SRP with parameter sets L1 and L2. The O-H-C angle was varied at the TS geometry (O-H-C = 180°) without partial optimization.

Table 4. PM3-SRP barriers ($\Delta E^{\ddagger}$) and reaction energies (ΔE_0), corrected for ZPE, compared to best estimates at 0 K (kcal/mol).

Reaction	□□□□□□ param. set L1		□□□□□□ param. set L2		Best estimate	
	$\Delta E^{\ddagger}$	ΔE_0	$\Delta E^{\ddagger}$	ΔE_0	$\Delta E^{\ddagger}$	ΔE_0
$O(^3P) + C_2H_6 \rightarrow OH + C_2H_5$	7.4	-3.7	7.1	-5.4	7 ± 1[a]	-5.5[d]
$OH + C_2H_6 \rightarrow H_2O + C_2H_5$	1.9	-18.6	1.9	-19.7	1 - 2[ab]	-21.3[d]
$OH + C_2H_5 \rightarrow H_2O + C_2H_4$	4.0	-15.3	2.6	-21.4	3.2[a]	-22.7[a]
$OH + C_2H_5 \rightarrow H_2O + CH_3CH$	1.0	-12.2	0.4	-14.8	3.8[a]	-14.4[a]
$O(^3P) + C_2H_6 \rightarrow CH_3O + CH_3$	38.7	-0.4	46.9	14.3	45.8[c]	-1.9[d]
$O(^3P) + C_2H_6 \rightarrow C_2H_5O + H$	44.2	22.0	49.7	41.1	50.5[c]	8.3[d]
$O(^3P) + C_3H_8 \rightarrow OH + n\text{-}C_3H_7$	7.5*	-4.7*	6.3*	1.9*	—	-5.4[d]
$O(^3P) + C_3H_8 \rightarrow OH + i\text{-}C_3H_7$	5.0*	-9.5*	4.4*	-1.3*	—	-8.2[d]

*Not included in the parametrization database.

[a]Yan, T.; Doubleday, C.; Hase, W. L. *J. Chem. Phys.* **120**, 9253-9265, (2004).

[b] Y.-Y. Chuang, C. Coitino, D. G. Truhlar, *J. Phys. Chem. A* **104**, 446 (2000).

[c] D. Troya, R. Pascual, D. J. Garton, T. Minton, and G. C. Schatz, *J. Phys. Chem. A* **107**, 7161 (2003).

[d]srdata.nist.gov/cccbdb, IV.A.1., experimental reaction data at 0 K.

Extensive optimizations of the tetramer yielded the global minimum in Figure 2. This structure maximizes the number of long range attractive H-H interactions.

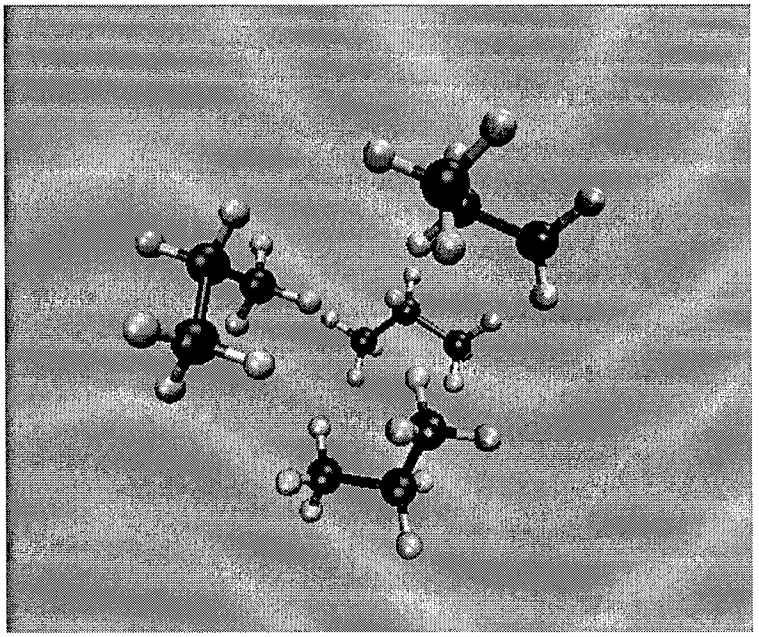

Figure 2. Optimized structure of propane tetramer.

Approximately 100000 trajectories were run with the L1 parameter set and 200000 with the L2 set. Initial conditions were selected and trajectories propagated using VENUS-MOPAC,[31] as described above for $O(^3P)$ + ethane. An important difference between trajectories run with the two parameter sets is the treatment of zero point energy. In trajectories run with the L1 set, vibrations are initialized with quasiclassical normal mode excitation. However, this may not give a realistic description of zero point energy. Since normal modes are delocalized and are initialized by superposition of randomly excited modes, the amount of energy placed in individual C-H bonds can deviate from the desired value by several kcal/mol, depending on the number of C-H bonds in the molecule. To produce a more realistic initial C-H vibrational distribution, we generalized the existing VENUS code for local mode excitation of a single vibration to allow all C-H bonds to be initialized as local modes instead of normal modes.

Quasiclassical local mode excitation gives each C-H bond the desired amount of energy, and was employed in all trajectories run with the L2 parameter set.

In all trajectories, reactants were initialized with a 298 K Boltzmann distribution of vibrational and rotational levels. For propane monomer, we examined collision energies E_{coll} = 8, 20, 40 kcal/mol (0.35, 0.87, 1.74 eV). For the tetramer, E_{coll} = 20, 40 kcal/mol, and only trajectories with zero impact parameter were examined.

At all collision energies, H-abstraction by O(^{3}P) constitutes 98-100% of the reaction, and the remainder involves H_2O formation from OH + C_3H_7. Figure 3 shows opacity functions for the monomer reactions at the three collision energies examined, for vibrational levels v = 0, 1, 2. The v = 0 level is dominant, in agreement with experiment.[33]

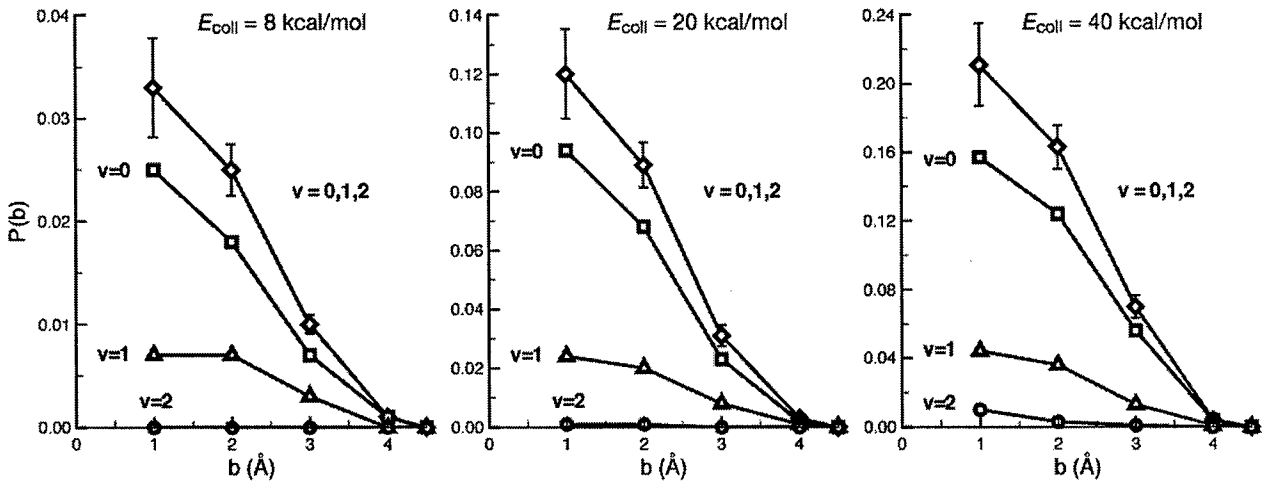

Figure 3. Opacity functions for reaction of O(^{3}P) with propane monomer at collision energies E_{coll} = 8, 20, 40 kcal/mol using the L2 parameter set. Impact parameter b is in Ångstroms.

A preference for secondary over primary C-H abstraction by O(^{3}P) is expected from the lower secondary barrier (Table 4). The results in Table 5 are consistent with this. In each case, the percent secondary is above the statistical value of 25%. The preference for secondary may be greater in the tetramer than the monomer, bu more trajectories would be needed to confirm this.

Table 5. Percent secondary C-H abstraction.

E_{coll}, kcal/mol	Monomer	Tetramer
8	37 ± 3	—
20	39 ± 3	43 ± 5
40	35 ± 3	37 ± 4

Angular distributions as measured by solid-angle differential cross sections vs cos(vv') are shown in Figures 4 (tetramer) and 5 (monomer). Here, v is the reactants' relative velocity vector pointing from O to C_3H_8, and v' is the relative velocity vector of the products pointing from C_3H_7 to OH. As expected for a nearly collinear transition state, back-scattering is dominant at low energy. For the monomer, forward scattering increases with increasing collision energy, consistent with a stripping mechanism.

Figure 6 compares the distribution of rotational levels j and vibrational levels v = 0, 1, 2, for trajectories run with parameter sets L1 and L2 at E_{coll} = 20 kcal/mol, and includes experimental results[33] for v = 0 (left plot, solid black circles). The important differences between the two sets of trajectories are that L2 includes the O-H-C bending data in Figure 1 while L1 does not, and that trajectories run with L2 are initialized with local mode C-H vibrational excitation. The OH P(v,j) distributions are clearly sensitive to the quality of the potential and the treatment of zero point energy. Trajectories based on the L2 parameter set, which are initialized with local mode C-H excitation, give much colder OH vibrational and rotational distributions, in agreement with the experimental distribution.[33]

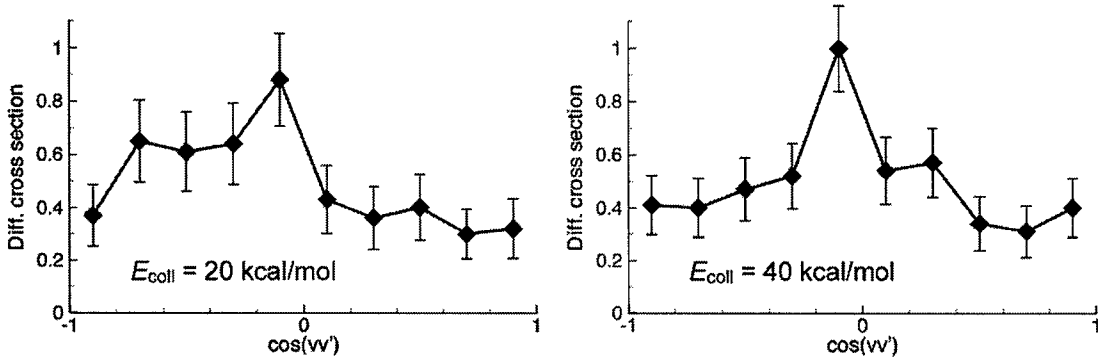

Figure 4. Normalized differential cross section $(1/\sigma)[\Delta\sigma/\Delta(\cos(vv'))]$ for tetramer reaction at zero impact parameter and collision energy E_{coll} = 20, 40 kcal/mol. v, v′ are initial and final relative velocity vectors. An interval $\Delta(\cos(vv')) = 0.2$ was used.

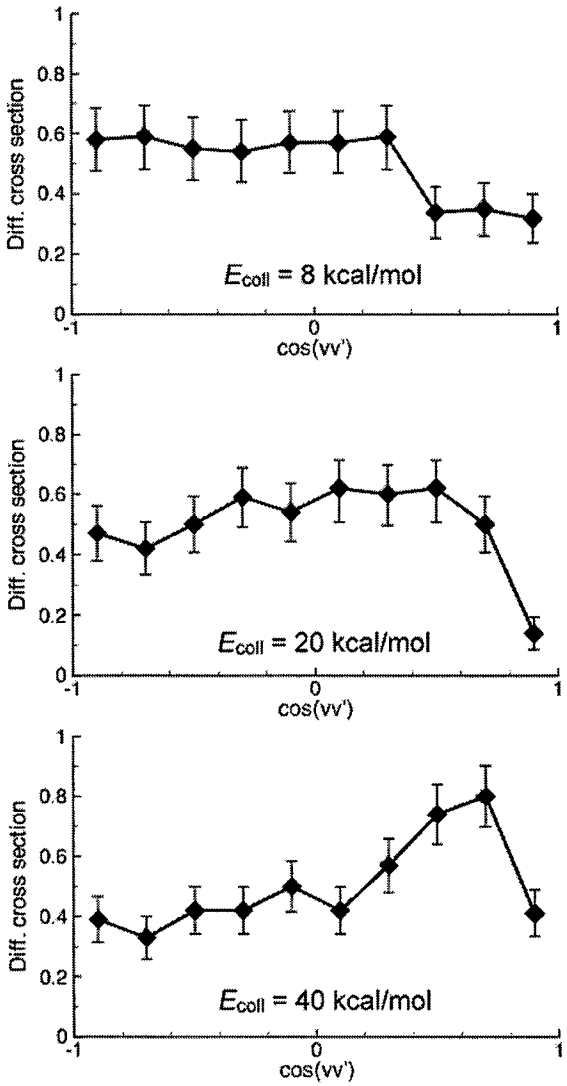

Figure 5. Normalized differential cross section $(1/\sigma)[\Delta\sigma/\Delta(\cos(vv'))]$ for monomer reaction at collision energy E_{coll} = 8, 20, 40 kcal/mol, where v, v′ are the initial and final relative velocity vectors. An interval $\Delta(\cos(vv')) = 0.2$ was used.

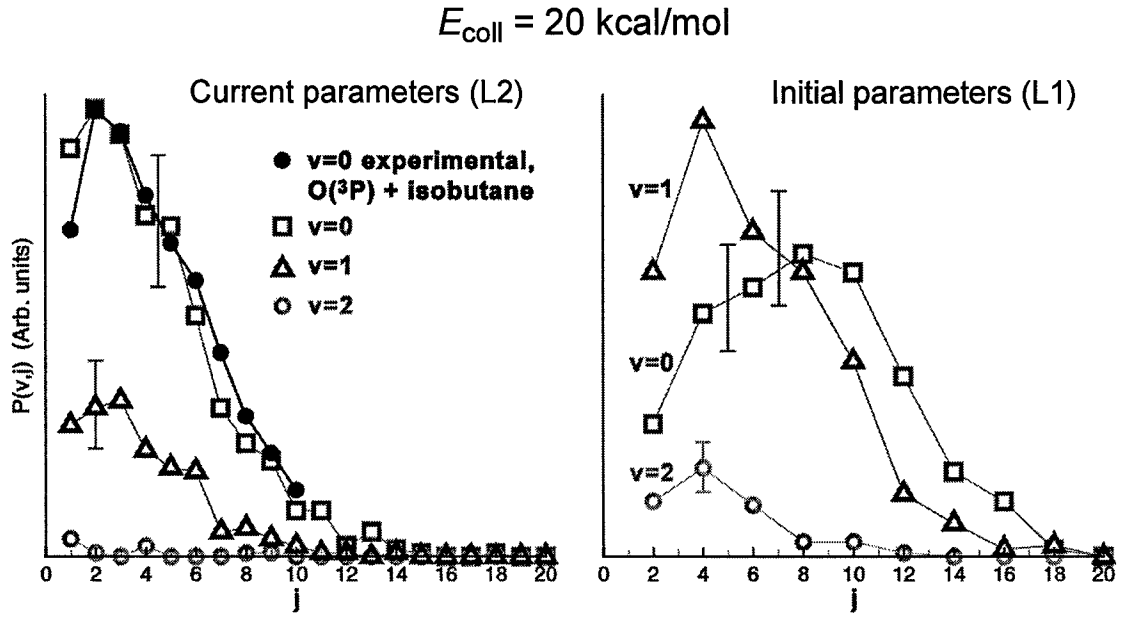

Figure 6. Vibration-rotation distributions of OH derived from $O(^3P)$ + C_3H_8 monomer with E_{coll} = 20 kcal/mol. P(v,j) is the probability of forming OH in vibrational state v and rotational state j. Typical error bars are shown. *Left:* the L2 parameter set was used, and trajectories were initialized with local mode C-H excitation. Exptl (black) from Ref. 33. *Right:* L1 parameter set and normal mode excitation.

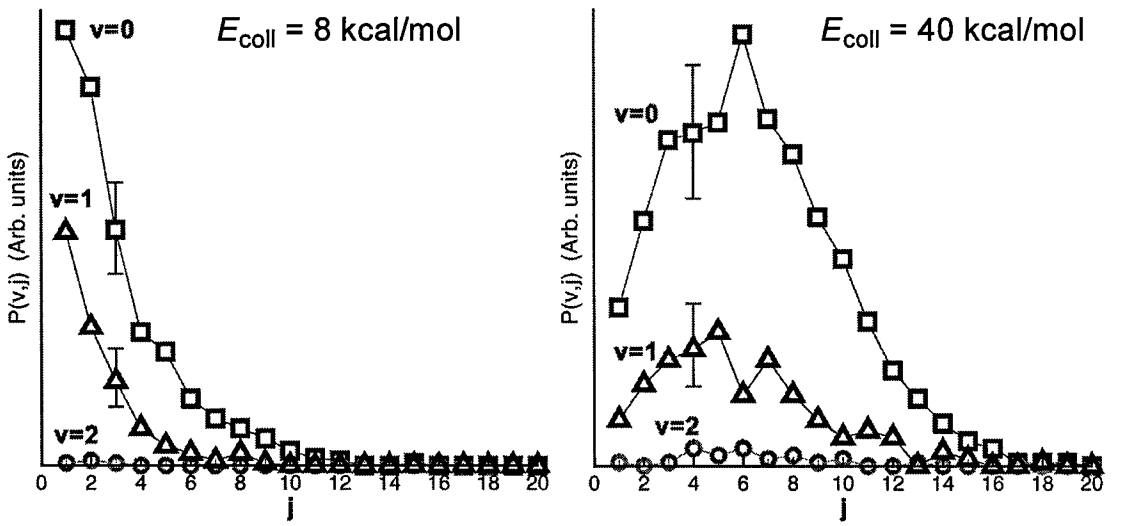

Figure 7. Vibration-rotation distributions of OH derived from $O(^3P)$ + C_3H_8 monomer with E_{coll} = 8 and 40 kcal/mol and the L2 parameter set. Typical error bars are shown.

Figure 7 shows analogous P(v,j) distributions for E_{coll} = 8 and 40 kcal/mol using the L2 parameter set and local mode C-H excitation. The rotational distribution shows the expected increase in the maximum of the distribution as E_{coll} increases. Figure 8 gives the P(v,j) distributions for OH product from O(^{3}P) + propane tetramer with E_{coll} = 20 and 40 kcal/mol with the L2 parameter set and local mode C-H excitation. Within the greater uncertainty due to fewer trajectories, the OH vibrational and rotational distributions derived from O(^{3}P) + tetramer are very similar to those produced from O(^{3}P) + monomer.

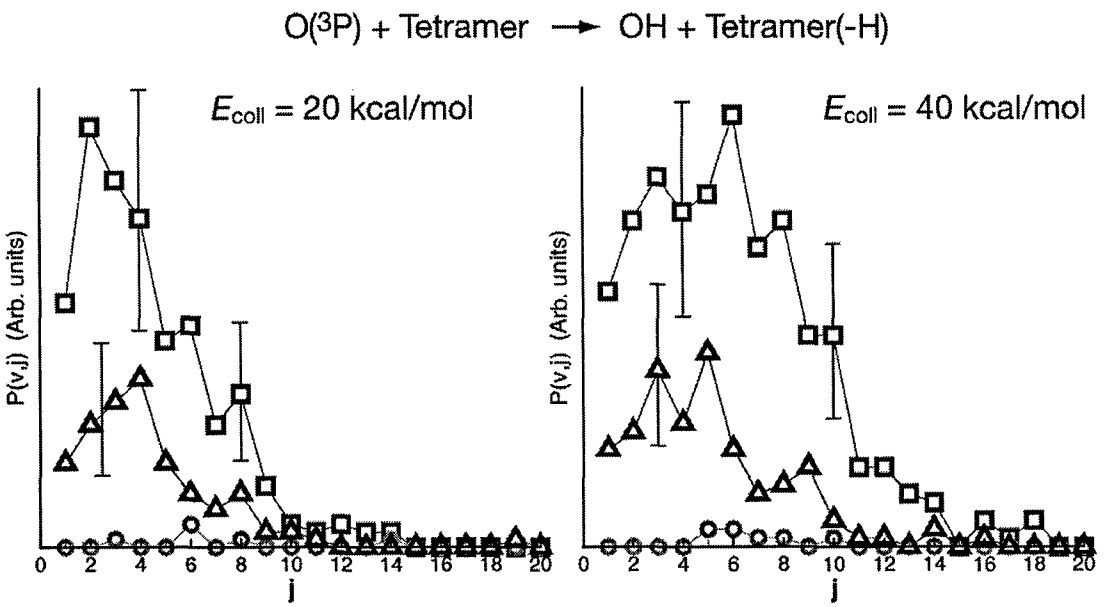

Figure 8. Vibration-rotation distributions of OH derived from O(^{3}P) + C_3H_8 tetramer with E_{coll} = 20 and 40 kcal/mol and the L2 parameter set. Typical error bars are shown.

Summary of O(3P) + propane. This work presents a PM3-SRP direct dynamics trajectory calculation of O(^{3}P) + propane monomer and tetramer reactions at low collision energies. The only important reaction at these energies is H-abstraction to form OH + propyl. Two parameter sets, L1 and L2, were created and extensive trajectories were run with each. In both parametrizations, the PM3-SRP potential reproduces the H-abstraction barriers very well, and the

reaction energetics somewhat less well. Inclusion of the O-H-C bending potential at the H-abstraction transition state in the ab initio database for the L2 set gives a PM3-SRP potential energy surface on which trajectories reproduce the cold OH rotational distribution observed experimentally (Figure 6).[33] Use of local mode C-H excitation gives propane the correct amount of initial zero point energy, and helps to reduce vibrational excitation in the OH product. The agreement with the experimental P(v,j) distribution suggests that the methods employed here are appropriate for reaction dynamics involving general hydrocarbon systems.

Dynamics of energy transfer and physisorption of O(^{3}P) atoms in collisions with alkane surfaces.

It is expected that the reactivity of O(^{3}P) atoms with hydrocarbon materials will be enhanced if a non-negligible fraction of the oxygen atoms physisorb on the material's surface. Adsorption will provide more time for O(^{3}P) to abstract an H-atom thus forming a hydroxyl radical, or provide more time for the triplet O(^{3}P)+alkane system to undergo intersystem-crossing to the much lower-energy singlet potential energy surface with the oxygen atom inserted into a C–H bond to form R–OH alcohol.

Minton and co-workers[8] have measured the translational energy distribution $P(E_f)$ for O(^{3}P) atoms scattered off 300 K liquid squalane at different incident energies E_i of 5.0, 11.2, 71.0 and 120.5 kcal/mol. For each of these E_i , there is a 300 K Boltzmann component in $P(E_f)$ suggesting that a fraction of the oxygen atoms are physisorbed and accommodated on (or in) the liquid squalane before desorbing with an energy distribution consistent with the liquid's 300 K temperature.

We have initiated an investigation of these experiments by first simulating inelastic collisions of O(^{3}P) with the $(C_{10}H_{21}S)_n$-Au (s) 1-decanethiol self-assembled monolayer

(H-SAM). Due to its homogeneity, this is a more straightforward surface to model than liquid squalane, and accordingly it is deemed to be most productive to initially probe the energy transfer and physisorption dynamics for $O(^3P)$ + H-SAM collisions.

Simulation Model and Potential Energy Function

The model used for the alkylthiolate H-SAM surface is the same as the one used in our previous studies of Ne atom scattering off this surface,[35,36] with the addition of periodic boundary conditions. At 300 K, the atoms of this surface have non-negligible thermal displacements, though the overall structure is still well-ordered. The following figure shows the height above the gold-plane vs. time (0-12 ps) of an H-atom attached to one of the surface's top

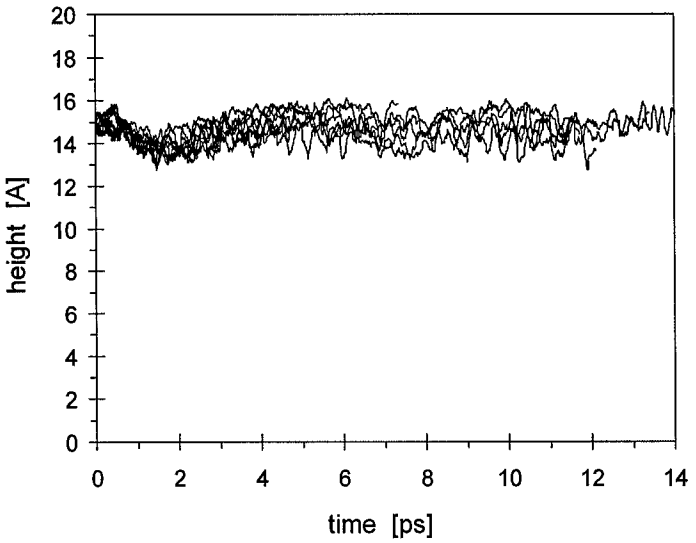

Figure 9. Plots of the surface's H atom's height above the gold plane as function of time for ten different trajectories.

methyl groups. This time dependence is plotted for ten different simulations. The plot shows that the surface atoms sit about 14.6±0.6 Å above the gold plane.

For the above simulations, the intermolecular potential between $O(^3P)$ and H-SAM is considered critical. A QM/MM model has been developed for modeling chemical reactions between $O(^3P)$ and H-SAM,[2,35,36,37] and at least one of these models[2] may accurately describe the intermolecular van der Waals interaction between oxygen and H-SAM. However, our calculations, which involve large ensembles of trajectories for many different incident energies and angles, are exceedingly computationally intensive and become impractical when the QM/MM model is used to provide the potential energy surface. Thus, the potential used here consists of analytic functions for the H-SAM and an analytic function for the oxygen + surface intermolecular interactions, written explicitly as a sum of two-body interaction terms between the oxygen and all the atoms of the surface. The parameters for this two-body potential function were determined by fitting three characteristic *ab initio* potential energy curves, calculated at the MP2/cc-pVTZ level of theory, for oxygen approaching CH_4 molecule in the face, edge and vertex orientations. The potential energy curve for the face orientation is shown in the figure below.

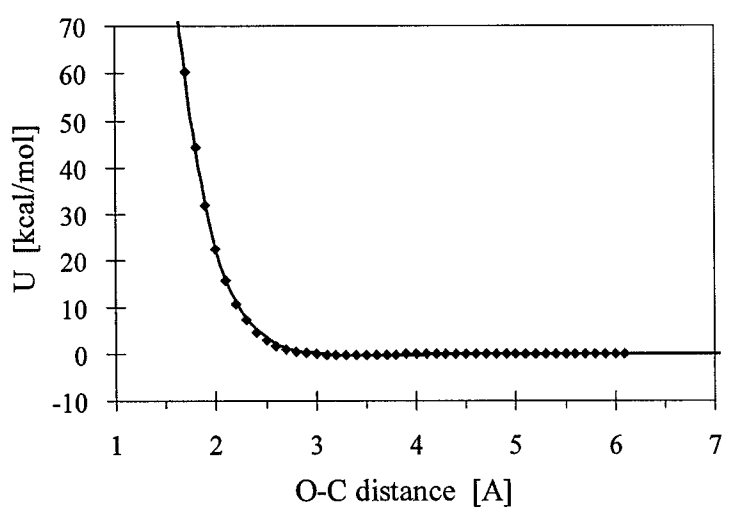

Figure 10. The MP2/cc-pVTZ potential energy curve for $O(^3P)$ + CH_4 in the face configuration. Red points are from the *ab initio* calculations, and the blue line is a fit.

The O–H and O–C two-body intermolecular potentials used to simultaneously fit all three *ab initio* curves are of the following form:

$$U(r) = a\,exp(-br) + c/r^6$$

The values of the fit parameters for all three orientations are given in the table below:

Table 1. Oxygen atom + methane intermolecular parameters

interaction	a [kcal/mol]	b [Å^{-1}]	c [mol kcal^{-1} Å^{-6}]
O–H	1070.7	3.191	-6.56
O–C	25106.4	3.324	-1044.36

This analytic potential gives respectively an O + CH_4 global potential energy minimum and O–C separation of -0.27554 kcal/mol and 3.499 Å for the face orientation, of -0.22756 kcal/mol and 3.635 Å for the edge orientation, and of -0.12705 kcal/mol and 4.086 Å for the vertex orientation. A previous crossed beam experimental study of O(^{3}P) + CH_4 scattering gave an average well-depth of -0.22 kcal/mol and 3.57 Å.[35] Due to a few trajectories in which the oxygen atom penetrates deep into the surface, we have also included O–S and O–Au interactions which are assumed to be repulsive-only and similar to O–C interactions.

Simulation Results

A Atomic-Level Dynamics

The following preliminary results are presented for simulation of O(^{3}P) + H-SAM collisions with a modest incident energy E_i of 2.30 kcal/mol, an incident angle θ_i of 60° to the surface normal, and a surface temperature T_{surf} of 300 K. The oxygen atom is assumed to begin

to significantly interact with the H-SAM surface when it is at 20 Å above the gold layer i.e. approximately 5.4 Å above the terminal $-CH_3$ groups. A similar criterion was used in the study of Ne + H-SAM inelastic scattering.[36] The minimum attained height of the oxygen atom approaching the gold surface is found to be always smaller than about 17.5 Å. The residence time of oxygen on the surface is thus calculated as the time period spent below the 20 Å mark. A wide range of residence times τ is observed: The oxygen atom may bounce back as quickly as its initial velocity allows it, with $\tau < 1$ ps, or it may linger on the surface for a considerable time, $\tau >$ 20 ps. Trajectories also exhibit a wide range in the number of oxygen-atom hops on the surface. Many trajectories finish with a single inner turning point, while others have multiple turning points, some in excess of 100, suggesting a long-term physisorption. The hops vary greatly both in timing and form. Some occur on the almost undetectable time-scale (< 0.02 ps) and with minute vertical displacements (< 0.001 Å), while others may involve long times (> 10 ps) and large vertical displacements (> 4 Å). Depths of oxygen penetration into the surface may differ greatly. The vast majority of oxygen atoms sample only the top few carbon layers of the surface, but a few penetrate deep into the surface, even hitting the bottom – the gold substrate. Some of these latter oxygen atoms appear to remain trapped inside the surface indefinitely, i.e. longer than 60 ps duration limit of the simulation. Approximately 2% of the oxygen atoms penetrate into H-SAM below an 11 Å height from the fixed gold surface. We may distinguish five types of trajectories: (*i*) vast majority (98%) sample the top of H-SAM surface only, not penetrating deeper than 13 Å, spending ~3.5 ps on the surface and having fewer than 20 hops. The other four types account for less than 1% each: (*ii*) trajectories that remain on the top of the H-SAM surface for a long time and experience numerous hops, (*iii*) trajectories that penetrate deep into the H-SAM but do not reach the Au(s) bottom before scattering off, (*iv*) trajectories that reach the

Au(s) bottom but eventually resurface back and scatter off, and (v) trajectories that remain trapped near the Au(s) bottom indefinitely. The ~1% of very deep-penetrating trajectories are associated with both long lifetimes and large numbers of hops (>20). Figures 11-16 illustrate some of the above-discussed collision dynamics.

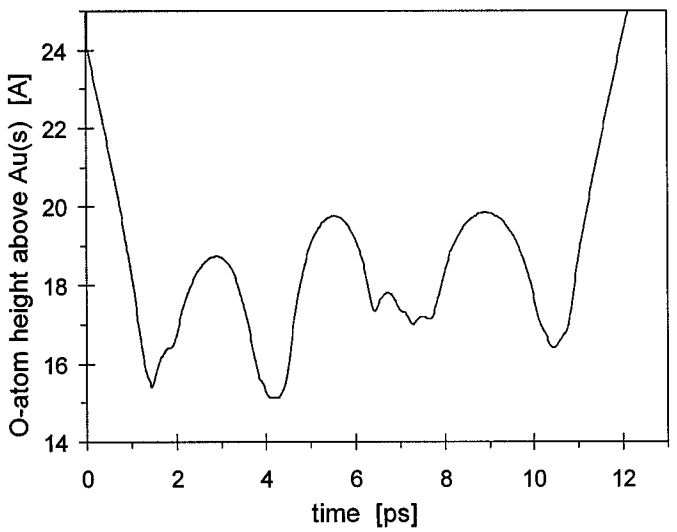

Figure 11. Plot of the oxygen atom height above Au(s) for a selected trajectory with multiple hops. The terminal methyl groups are located at ~14.6 Å. This oxygen atom remains near the surface top at all times.

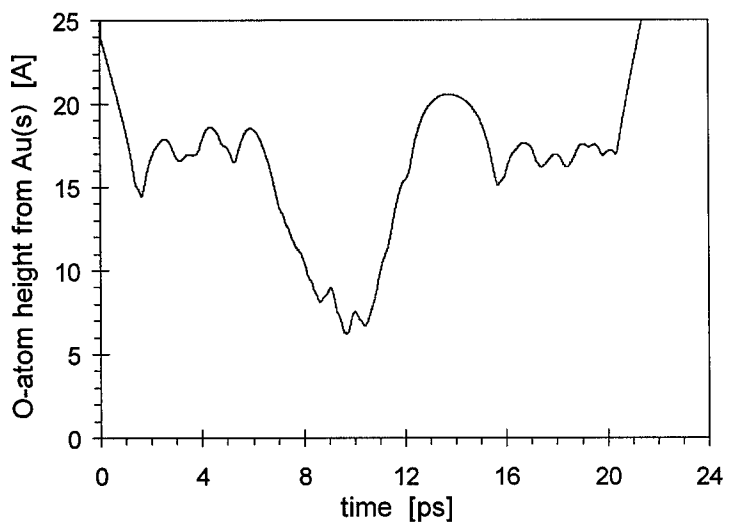

Figure 12. Plot of the oxygen atom height above Au(s) for a trajectory with deep penetration. The atom reaches half-way down through the surface, but manages to desorb within 20 ps.

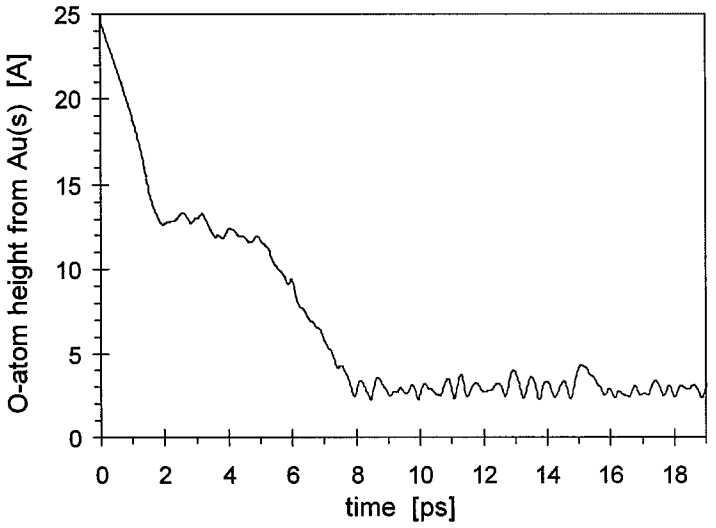

Figure13. Plot of the oxygen atom height above Au(s) for a trajectory which becomes caught in the region between Au(s) and the last/bottom carbon atom of the alkyl chain. The oxygen does not escape during the simulation's duration. This is an example of very strong physisorption.

Individual trajectories are not very informative nor representative, and thus it is of interest too look at statistics of selected trajectory characteristics. In the Figures 14-16 are shown probability distributions for some of the significant gas+surface collision aspects from a set of 500 trajectories.

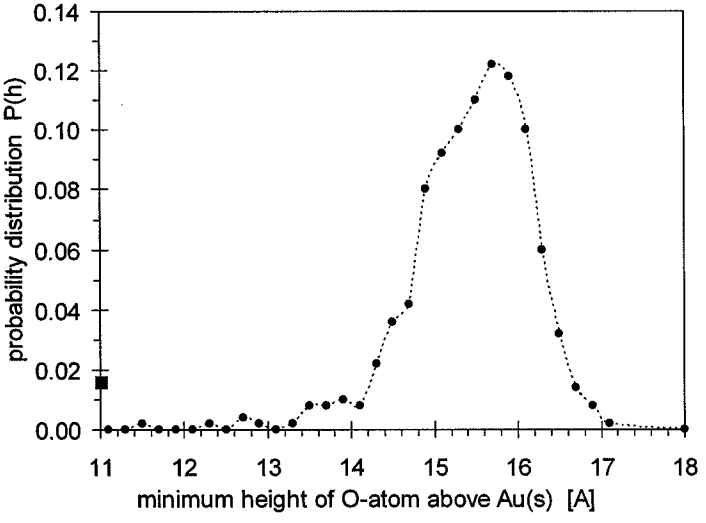

Figure 14. Distribution of the minimum oxygen height above Au(s) for the trajectories.

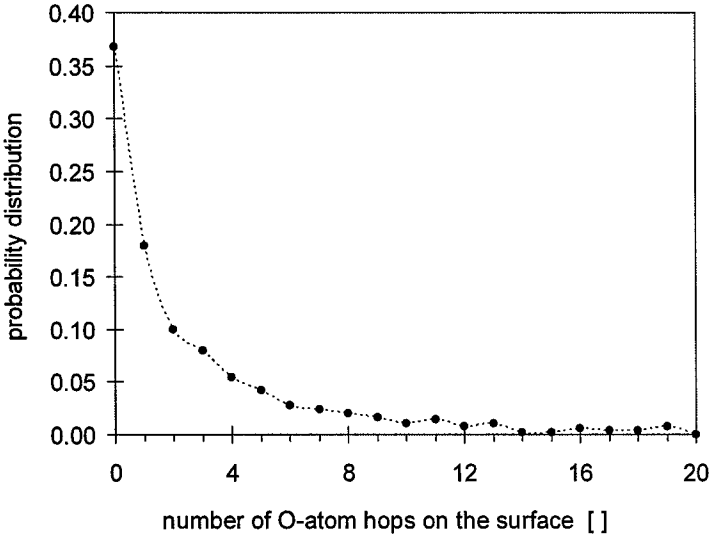

Figure 15. Distribution of the number of hops that oxygen atom executes on the H-SAM/Au(s) surface.

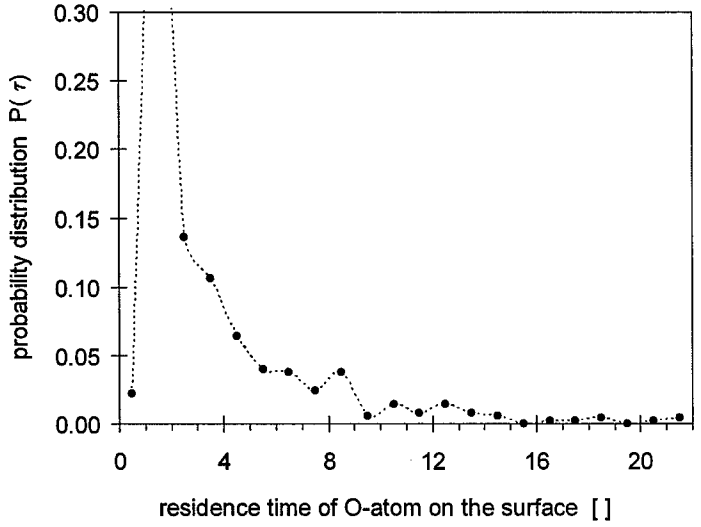

Figure 16. Distribution of the oxygen residence time on the H-SAM/Au(s) surface.

B Correlations Between Dynamic Characteristics

While dynamic characteristics of individual trajectories differ widely as described by the above distributions, there are some important correlations between certain characteristics of the $O(^3P)$ + H-SAM collisions. These characteristics: the smallest height reached throughout trajectory, total number of hops, total residence time, the final translational energy etc., are

different ways of describing already completed trajectories, and may have parallel trends, but cannot be clearly assigned any causal-consequential relationships i.e. dependencies. It is of particular interest to determine how the final translational energy E_f of the outgoing oxygen associates with various attributes of the collision dynamics.

In the following figures, some of these correlations are presented in the form of scatter plots. Figures 17 and 18 show links between E_f and the number of hops, and between E_f and the residence time, respectively. In collisions with no or few hops, the oxygen atom may transfer anything from a small to large energy to the surface, while trajectories with many hops tend to end with departing oxygen leaving behind the excess of its initial energy. The E_f values for collisions with E_i = 2.30 kcal/mol and with a single inner turning point, vary from near zero (elastic) to almost 6 kcal/mol, illustrating that in some collisions thermal energy of H-SAM may even be deposited into the oxygen atom. However, in most trajectories the energy is of course taken away from the hotter oxygen. Although the statistics is not good enough with the currently available data, there are indications that an increasing net energy transfer occurs for trajectories with more hops i.e. that oxygen atoms that ramble more on the surface are better thermalized, as one would indeed expect. Additional data are nevertheless needed to secure and quantify this relationship. Furthermore, collisions with larger initial energy E_i are expected to show this relationship more prominently. The trajectories with extraneously large number of hops are those that remain adsorbed on the surface, and are not included in the figures below.

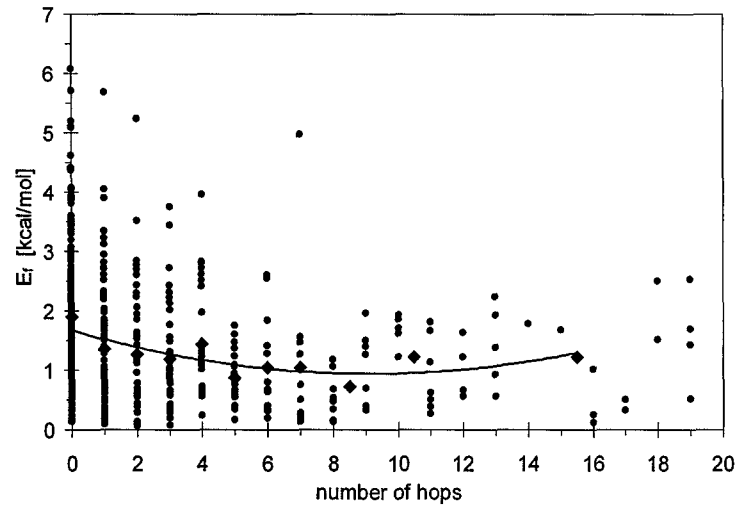

Figure 17. Scatter plot of 490 trajectories illustrating that the average final oxygen translational energy $\langle E_f \rangle$ (blue line) decreases as the number of hops increases.

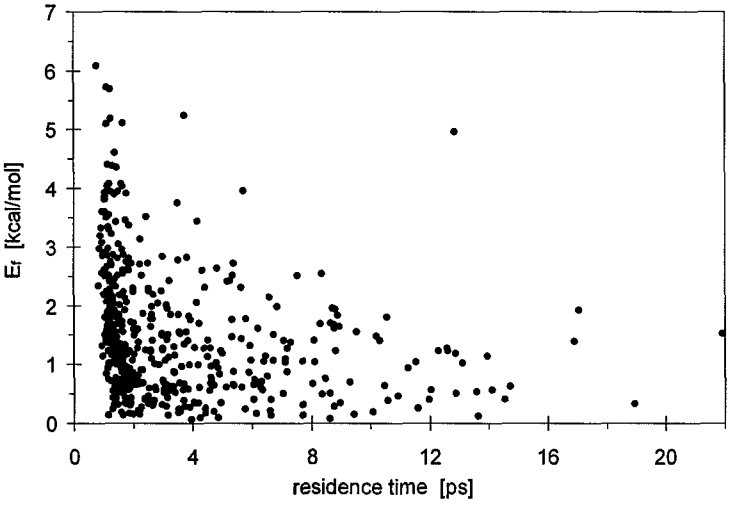

Figure 18. Scatter plot of the same trajectories as in Fig.17 illustrating similarly that the final oxygen energy $\langle E_f \rangle$ tends to be small for trajectories with longer residence times.

For the vast majority of trajectories, there is no noticeable correlation between the depth to which the oxygen atom penetrates the H-SAM surface and the oxygen final translational energy. It appears that the energy with which oxygen is scattered off the surface probably depends primarily on the last few moments of its residence, just before its take-off, and that the region where oxygen previously roamed in the surface i.e. close to the surface top or deep inside,

is not very significant except in the sense that it might tend to be associated with different residence times. There is a weak positive link between the maximum depth of penetration (minimum reached height) and the residence time. Indeed, in the few available trajectories with deep penetration, oxygen does not leave surface with large E_f. It should be noted, however, that all these energies involved in present calculations are rather small. For those few trajectories which remain adsorbed on the surface, there clearly can be no E_f value.

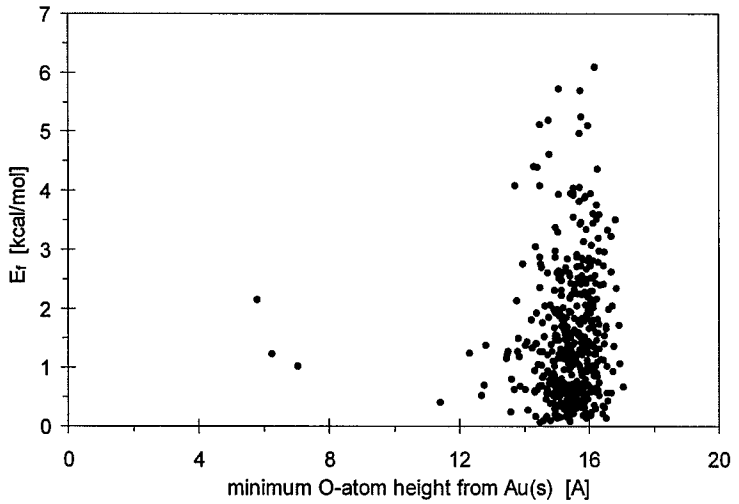

Figure 19. Scatter plot of the same trajectories as in Fig.17 illustrating little link between the final oxygen translational energy and the minimum height.

In Figure 19, a correlation may be hidden or obscured by the generally large scatter and by the fact that few trajectories venture deep into H-SAM. The existing scatter of data-points represents the intrinsic uncertainty and natural variability in trajectory outcomes, rather than a computational random error, of which there is none.

Similarly, there is no noticeable correlation between the number of hops and the greatest depth of penetration. In other words, the oxygen atom may bounce around equally well in any region of the surface, in the top as well as in the lower layers of the surface, as shown in Figure 20. Presumably, the depth of penetration is determined primarily by the relative surface geometry.

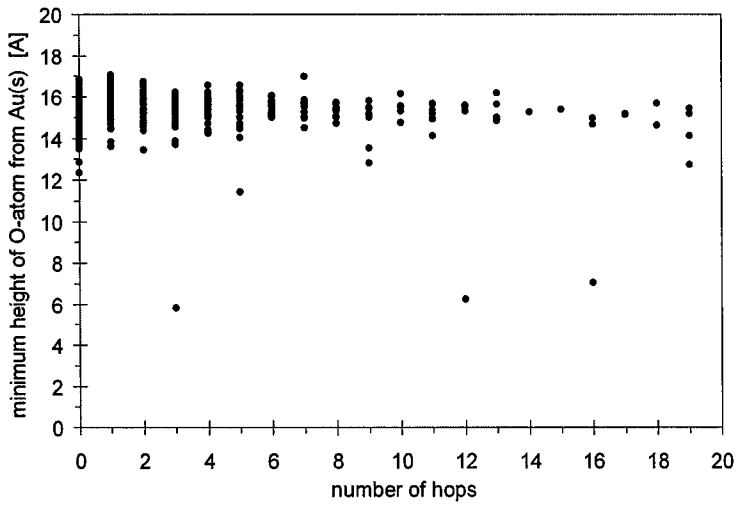

Figure 20. Relationship between the number of hops and the depth of penetration.

C Translational Energy and Scattering Angle Distributions

The distribution of the final translational energies of the scattered oxygen atom is shown in Figure 13, where it is compared to the 300 K distribution for thermal desorption. The initial trajectory conditions are the same as above: E_i = 2.30 kcal/mol, θ_i = 60° and T_{surf} = 300 K. The $P(E_f)$ apparently has a significant non-thermal component. With an appropriate convention, it should be possible to de-convolute the Boltzmann (BC) and the non-Boltzmann (NB) contributions when more trajectories become available i.e. when the distribution becomes better resolved.

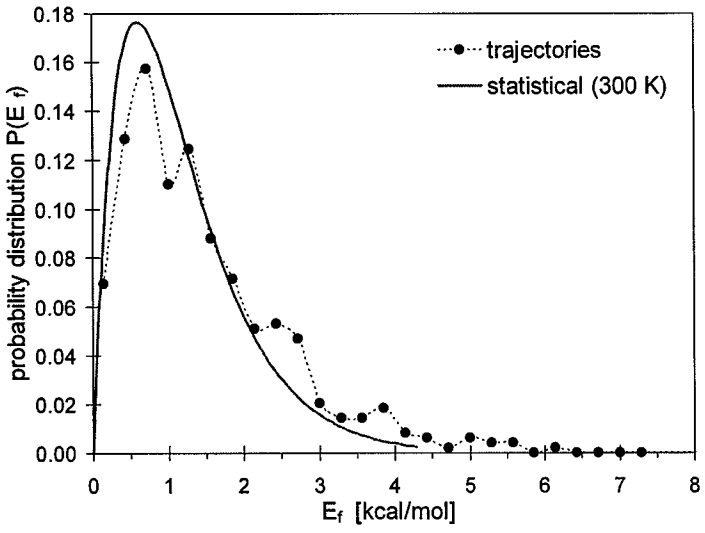

Figure 21. Two distributions of the final translational energies of the scattered oxygen atom: from the trajectory calculations (points) and statistical from thermal desorption (line).

The probability distribution of the polar angle θ_f of the outgoing, scattered oxygen atom is shown in Figure 14. The initial (incoming) θ_i and final (outgoing) θ_f angles are both defined as the angle between oxygen velocity and the surface normal long before and long after collision, respectively. The average outgoing angle $\langle\theta_f\rangle$ is 47°, smaller than the incoming fixed angle θ_i = 60°.

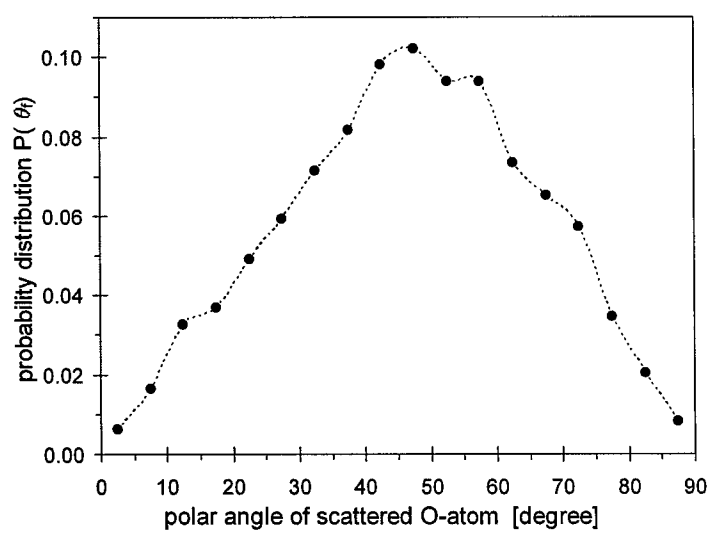

Figure 22. Distribution of the scattering angle θ_f of the oxygen atom.

D Comparison of Results for Different Incident Angles

The above discussion and figures pertain to the atomic-level dynamics of $O(^3P)$ collisions at $E_i = 2.30$ kcal/mol and $\theta_i = 60°$ with H-SAM. Additionally, we have performed analogous sets of trajectories with a range of initial, incident polar angles: $\theta_i = 15°$, 30°, 45° and 75°. Each set contains about 500 trajectories. Most of the trajectory properties have been found to be very similar, and without any strong dependence on θ_i except for the minimum height of the oxygen atom from Au(s), suggesting that more slanted collisions tend to penetrate slightly deeper than the more orthogonal ones. An interesting finding is that regardless of the incoming angle θ_i, the outgoing angle θ_f is about 45°, suggesting that the tilt and orientation of the alkane chains determines the scattering angle.

The findings for all incident angles, and for trajectories that end up with the oxygen atom escaping from the surface, may be summarized as following: the average final energy $\langle E_f \rangle$ = 1.5±1 kcal/mol, the average scattering polar angle $\langle \theta_f \rangle$ = 45°±20°, the average residence time $\langle t_{res} \rangle$ = 4±4 ps, the average minimum depth of penetration $\langle h_{min} \rangle$ = 15±2 Å, and the average number of hops $\langle N_{hops} \rangle$ = 3±4. In all cases, the $P(E_f)$ distribution has a significant Boltzmann component, but is still clearly non-statistical. Analysis is under way to quantify the fraction and characteristics of the non-Boltzmann contributions that can be compared with the experiments.[8]

The lack of significant systematic and obvious distinctions among trajectory sets with different incident angles may be due to several factors: these preliminary data may not provide sufficiently good statistics, or the differences may be very subtle compared to intrinsic variability for any simple comparison. Also, the corrugation and complexity of the H-SAM surface structure may lead to non-trivial angular dependence. Finally, it may be that only the direct

collisions, with no turning points, would preserve correlation between the incident angle and the final trajectory characteristics such as the scattering translational energy E_f. Further studies are under way to explore these issues, as well as to extend these simulations to higher, more relevant energies. It is suspected that some of the trends, probability distributions and correlations might become more well-defined, definite and distinct as one probes the highly energized $O(^3P)$ atoms.

Extensions to $O(^3P)$ + Liquid Squalane

In simulations that are being initiated at this time, the above studies will be extended to $O(^3P)$ inelastic and reactive scattering off liquid squalane.

References

1. T. Yan, W. L. Hase, and C. Doubleday, *J. Chem. Phys.* **120**, 9253-9265 (2004).
2. T. Yan, C. Doubleday, and W. L. Hase, *J. Phys. Chem. A* **108**, 9863-9875 (2004).
3. C. Doubleday, presented at AFOSR contractor's meeting, 5/23/05, Monterey, CA. Manuscript in preparation.
4. U. Tasic, T. Yan, and W. L. Hase, *J. Phys. Chem. B* **110**, xxxx-xxxx (2006).
5. P. Andresen and A. C. Luntz, *J. Chem. Phys.* **72**, 5842 (1980).
6. F. Ausfelder and K. G. McKendrick, *Prog. Reac. Kinet. Mech.* **25**, 299 (2000).
7. H. Tsurumaki, Y. Fujimura, and O. Kajimoto, *J. Chem. Phys.* **112**, 2000 (2000).
8. D. J. Garton, T. K. Minton, M. Alagia, N. Balucani, P. Casavecchia, and G. G. Volpi, *Faraday Discuss. Chem. Soc.* **108**, 387 (1997); J. Zhang, D. J. Garton, and T. K. Minton, *J. Chem. Phys.* **117**, 6239 (2002).
9. A. Migoshi, K. Tsuchiya, N. Yamauchi, and H. Matsui, *J. Phys. Chem.* **98**, 11452 (1994).
10. D. L. Baulch, C. J. Cobos, R. A. Cox, C. Esser, P. Frank, T. Just, J. A. Kerr, M. J. Pilling, J. Troe, R. W. Walker, and J. Warnatz, *J. Phys. Chem. Ref. Data* **21**, 411 (1992).
11. N. Cohen and K. R. Westberg, *J. Phys. Chem. Ref. Data* **20**, 1211 (1991).
12. J. C. Corchado, J. Espinosa-Garcia, O. Roberto-Neto, Y.-Y. Chuang, and D. G. Truhlar, *J. Phys. Chem. A* **102**, 4899 (1998).
13. T. P. Nguyen, A. Lahmar, and P. Jonnard, J. Adhesion **66**, 303 (1998); M. S. Hartney, D. W. Hess, and D. S. Soane, J. Vac. Sci. Technol. **B7**, 1 (1989); O. Joubert, J. Pelletier, and Y. Arnal, *J. Appl. Phys.* **65**, 5096 (1989); C. M. Chan, T. M. Ko, and H. Hiraoka, *Surf. Sci. Rep.* **24**, 1 (1996).
14. T. K. Minton and D. J. Garton, in *Chemical Dynamics in Extreme Environments*, edited by R. A. Dressler (World Scientific, Singapore, 2001), pp. 420; E. Grossman and I. Gouzman, Nucl. Instruments Methods Phys. Res. B **208**, 48 (2003).
15. D. J. Garton, T. K. Minton, M. Alagia, K. Balucani, P. Casavecchia, and G. G. Volpi, J. Chem. Phys. **112**, 5975 (2000).
16. T. K. Minton, J. Zhang, D. J. Garton, and J. W. Seale, High Performance Polymers **12**, 1 (2000); H. Kelso, S. P. K. Kohjer, D. A. Henderson, and K. G. McKendrick, presented at the the 19th Conference on the Dynamics of Molecular Collisions, 2003 (unpublished).
17. G. Li, S. B. M. Bosio, and W. L. Hase, *J. Mol. Struct.* **556**, 43 (2000).
18. D. Troya, R. Z. Pascual, and G. C. Schatz, *J. Phys. Chem. A*, **107**, 10497 (2003).
19. D. Troya, R. Z. Pascual, D. J. Garton, T. K. Minton, and G. C. Schatz, *J. Phys. Chem. A* **107**, 7161 (2003).
20. A. Gindulyte, L. Massa, B. A. Bands, and S. K. Rutledge, *J. Phys. Chem. A* **104**, 9976 (2000).
21. D. J. Garton, T. K. Minton, D. Troya, R. Pascual, and G. C. Schatz, *J. Phys. Chem. A* **107**, 4583 (2003).
22. H.-J. Werner and P. J. Knowles, J. Chem. Phys. **82**, 5053 (1985); P. J. Knowles and H.-J. Werner, *Chem. Phys. Lett.* **115**, 259 (1985).
23. H.-J. Werner, *Mol. Phys.* **89**, 645 (1996).
24. P. Celani and H.-J. Werner, *J. Chem. Phys.* **112**, 5546 (2000).
25. H.-J. Werner and P. J. Knowles, *J. Chem. Phys.* **89**, 5803 (1988); P. J. Knowles and H.-J. Werner, *Chem. Phys. Lett.* **145**, 514 (1988).

26. MOLPRO, a package of ab initio programs designed by H. -J. Werner and P. J. Knowles, version 2002.3 (2002). R. D. Amos, A. Bernhardsson, A. Berning, P. Celani, D. L. Cooper, M. J. O. Deegan, A. J. Dobbyn, F. Eckert, C. Hampel, G. Hetzer, P. J. Knowles, T. Korona, R. Lindh, A. W. Lloyd, S. J. McNicholas, F. R. Manby, W. Meyer, M. E. Mura, A. Nicklab P. Palmieri, R. Pitzer, G. Rauhut, M. Schütz, U. Schumann, H. Stoll, A. J. Stone, R. Tarroni, T. Thorsteinsson, and H.-J. Werner.
27. M. W. Schmidt, K. K. Baldridge, J. A. Boatz, S. T. Elbert, M. S. Gordon, J. H. Jensen, S. Koseki, N. Matsunaga, K. A. Nguyen, S. Su, T. L. Windus, M. Dupuis, and J. J. A. Montgomery, *J. Comput. Chem.* **14,** 1347 (1993).
28. A. Halkier, T. Helgaker, P. Jorgensen, W. Klopper, H. Koch, J. Olsen, and A. K. Wilson, *Chem. Phys. Lett.* **286,** 243 (1998).
29. Stewart, J. J. P. *J. Comput. Chem.* **209**, 10 (1989).
30. Press, W. H.; Teukolsky, S. A.; Vetterling, W. T.; Flannery, B. P. *Numerical Recipes in Fortran*; Cambridge University Press, 1992.
31. G. H. Peslherbe, K. Bolton, C. Doubleday, and W. L. Hase, VENUS-MOPAC, a General Chemical Dynamics and Semiempirical Direct Dynamics Computer Program. To be released.
32. Hase, W. L.; Duchovic, R. J.; Hu, X.; Kormonicki, A.; Lim, K.; Lu, D.-H.; Peslherbe, G. H.; Swamy, K. N.; Linds, S. R. V.; Varandos, A. J. C.; Wang, H.; Wolf, R. J. QCPE 1996, 16, 671.
33. G. M. Sweeney, A. Watson, and K. G. McKendrick, *J. Chem. Phys.* **106**, 9172 (1997).
34. Y. Zhao, B. J. Lynch, and D. G. Truhlar *J. Phys. Chem. A* **108**, 2715 (2004).
35. T.-Y. Yan, N. Isa, K. D. Gibson, S. J. Sibener and W. L. Hase *J. Phys. Chem. A* **107**, 10600 (2003).
36. N. Isa, K. D. Gibson, T.-Y. Yan, W. L. Hase and S. J. Sibener: *J. Chem. Phys.* **120**, 2417 (2004).
37. (a) G. Li, S. B. M. Bosio and W. L. Hase: *J. Molec. Struc.* **556**, 43 (2000). (b) D. Troya and G. C. Schatz: *J. Chem. Phys.* **120**, 7696 (2004).

APPENDIX
PM3-SRP parameter sets L2 and L2 for O(^{3}P) + propane

Table A1. Parameters for $V_{analytical}$, eq 2.

	Parameter set L1		Parameter set L2	
	O-C	O-H	O-C	O-H
a	11292.12193	7808.19694	11304.51802	7296.17834
b	3.64224	3.86856	3.72843	3.84999
c	-509.06505	-126.28879	-435.41934	-109.08288
f	16.36333	20.76417	19.19875	27.93941
r_0	2.52666	2.96078	2.49297	3.01180

Table A2. Conventional PM3 parameters of $V_{PM3\text{-}SRP}$.

		Original PM3	Parameter set L1	Parameter set L2
H	α	3.356386	3.553597	3.633979
H	**U***ss*	-13.073321	-12.881635	-12.757258
H	**G***ss*	14.794208	14.930383	14.777858
H	β*s*	-5.626512	-6.034970	-5.950367
H	ζ*s*	0.967807	.958627	.920356
C	α	2.707807	2.629564	2.571816
C	**U***ss*	-47.270320	-47.073019	-46.112978
C	**U***pp*	-36.266918	-35.551186	-35.647445
C	**G***ss*	11.200708	12.209925	11.785205
C	**G***sp*	10.265027	10.191357	10.370604
C	**G***pp*	10.796292	10.932203	10.853004
C	**G***p*2	9.042566	8.756955	8.653818
C	**H***sp*	2.290980	2.351730	2.344364
C	β*s*	-11.910015	-11.251613	-11.380953
C	β*p*	-9.802755	-9.413070	-9.744799
C	ζ*s*	1.565085	1.612331	1.581688
C	ζ*p*	1.842345	1.818345	1.797398
O	α	3.217102	3.196680	3.191208
O	**U***ss*	-86.993002	-100.004064	-97.929636
O	**U***pp*	-71.879580	-71.349149	-70.501462
O	**G***ss*	15.755760	16.406318	16.447563
O	**G***sp*	10.621160	12.384200	12.052675
O	**G***pp*	13.654016	14.292968	14.129753
O	**G***p*2	12.406095	11.281769	11.051201
O	**H***sp*	0.593883	.682771	.669554
O	β*s*	-45.202651	-45.666997	-46.768261
O	β*p*	-24.752515	-24.644967	-25.440923
O	ζ*s*	3.796544	3.949335	3.818890
O	ζ*p*	2.389402	2.413209	2.517966

Table A3. Parameters of $V_{PM3\text{-}SRP}$ associated with eq 3 and 4, parameter set L1.

	OH_1	OH_2	CH	CO	CC	HH
$\chi^{ss}_{ij,small}$	0.96737	0.96737[a]	1.00334	1.03712	.99433	.63892
$\chi^{ss}_{ij,large}$	1.02716	1.05424	0.98535	1.29202	1.10754	1.39063
$\chi^{sp}_{ij,small}$	0.95147	0.95147[a]	1.00561	1.01078	1.05909	
$\chi^{sp}_{ij,large}$	1.06693	1.06298	1.01144	1.48728	1.27403	
$\chi^{pp}_{ij,small}$				1.03484	1.06301	
$\chi^{pp}_{ij,large}$				1.23265	1.30648	
f_{ij}	3.81972	3.85625	3.06940	2.79345	2.70682	4.09569
r^0_{ij}	1.08632	1.06250	1.53273	2.45222	1.99144	3.34919

[a] Identical to OH_1 parameter (not independent).

Table A4. Parameters of $V_{PM3\text{-}SRP}$ associated with eq 3 and 4, parameter set L2.

	OH_1	OH_2	CH	CO	CC	HH
$\chi^{ss}_{ij,small}$	0.944234	0.944234[a]	1.041469	1.056987	1.030936	0.581784
$\chi^{ss}_{ij,large}$	1.069680	1.067088	0.977619	1.289147	1.131113	1.343868
$\chi^{sp}_{ij,small}$	0.932780	0.932780[a]	1.006816	1.017941	1.039463	
$\chi^{sp}_{ij,large}$	1.095890	1.056415	1.025879	1.431303	1.284242	
$\chi^{pp}_{ij,small}$				1.012786	1.067242	
$\chi^{pp}_{ij,large}$				1.203813	1.368468	
f_{ij}	3.703252	3.811209	3.081621	2.783867	2.725377	4.095683
r^0_{ij}	1.120038	1.052181	1.484811	2.402244	1.974958	3.333669

[a] Identical to OH_1 parameter (not independent).

Personnel Supported:

Dr. Charles Doubleday, Department of Chemistry, Columbia University
Dr. Uros Tasic, Department of Chemistry and Biochemistry, Texas Tech University

Publications:

T. Yan, W. L. Hase, and C. Doubleday, "Energetics, transition states, and intrinsic reaction coordinates for reactions associated with $O(^3P)$ processing of hydrocarbon materials," *J. Chem. Phys.* **120**, 9253-9265 (2004).

T. Yan, C. Doubleday, and W. L. Hase, "A PM3-SRP + Analytic Function Potential Energy Surface Model for $O(^3P)$ Reactions with Alkanes. Application to $O(^3P)$ + Ethane" *J. Phys. Chem. A* **108**, 9863-9875 (2004).

U. Tasic, T. Yan, and W. L. Hase, "Dynamics of Energy Transfer in Collisions of $O(^3P)$ Atoms with a 1-Decanethiol Self-Assembled Monolayer Surface," *J. Phys. Chem. B* **110**, xxxx-xxxx (2006).

C. Doubleday, and W. L. Hase, "Dynamics of $O(^3P)$ Reaction with Propane and Propane Tetramer," in preparation.

Interactions/Transitions:

Meetings:

Presented in part at the following AFOSR Contractors Meetings:

May 18-21, 2003, San Diego, CA.
May 24-26, 2004, Newport, RI.
May 22-24, 2005, Monterey, CA.

19th Conference on the Dynamics of Molecular Collisions, Granlibakken Conference Center at Lake Tahoe, California (July 13-18, 2003)
"Dynamics of Energy Transfer and Chemical Reaction in Gas-Surface Collisions"

TACC-2004, Theory and Applications of Computational Chemistry, Gyeongju, Korea (February 15-20, 2004)
"Studying Microscopic Reaction Mechanisms by QM, QM+MM, and QM/MM Direct Dynamics Simulations"

227th ACS National Meeting, Symposium on Computational Approaches to Problems in Environmental Chemistry, Anaheim, California (March 29 – April 1, 2004)
"Energy Transfer and Chemical Reaction in Collisions of Rare Gas and Triplet Oxygen Atoms with Hydrocarbon Surfaces"

227th ACS National Meeting, Symposium on Mixed Quantum, Classical and Semi-classical Dynamics, Anaheim, California (March 29 – April 1, 2004)
"Applications of QM, QM+MM, and QM/MM Direct Dynamics Simulations"

West Texas Nanotechnology Forum, Lubbock, Texas, April 19, 2005, W. L. Hase, "VENUS. A Computer Program for Simulating Atomic-Level Motions and Properties of Nanomaterials".

230th ACS National Meeting, Symposium on Applications of Self-Assembled Monolayers (SAMs) in Surface and Interface Science, Washington D. C., August 28-September 1, 2005, W. L. Hase, "Chemical Dynamics Simulations of Energy Transfer and Reaction in Collisions of Projectiles with Self-Assembled Monolayers".

Seminars by W. L. Hase at Universities: Washington University, Chemistry (November 5, 2002); Texas Tech University, Chemistry (January 23, 2003); Wayne State University, Computer Science (March 18, 2003); Virginia Tech University, Chemistry (August 29, 2003); Wayne State University, Physics (September 16, 2003); Kalamazoo College, Chemistry (November 3, 2003); Korea National University of Education, Chemistry (February 13, 2004); Nagoya University, Institute for Scientific Computing (February 23, 2004); Texas Tech University, Chemistry (March 12, 2004); Michigan State University, Chemistry (April 15, 2004); Baylor University, Chemistry (November 5, 2004); Texas Tech University, Mathematics (November 18, 2004); University of Maryland, Center for Scientific Computation and Mathematical Modeling (February 16, 2005); University of North Texas, Chemistry (May 6, 2005); University of New Mexico, Chemistry (September 23, 2005); Texas Tech University, Physics (November 10, 2005).

Consultative and Advisory Functions:
Bill Hase has discussed $O(^3P)$ chemical dynamics with Robert Shroll at Spectral Sciences, Inc.

Bill Hase participated in the STTR proposal, "Computational Prediction of Kinetic Rate Constants", with Robert Shroll from Spectral Sciences, Inc.as the PI. This proposal was recommended for Phase I funding.

Transitions:
We have discussed the use of our computer program package VENUS/MOPAC, with Robert Shroll at Spectral Sciences, Inc. He would use the program to study the reaction of $O(^3P)$ atoms with alkane molecules and surfaces.

We have developed the website **cdssim.chem.ttu.edu** for distributing our software.

New Discoveries, Inventions, or Patent Disclosures: None.

Honors/Awards:
a. William L. Hase
Fellow in the American Physical Society, 1991

Elected to Lifetime Membership in the Academy of Scholars of Wayne State University, 1994

Fellow in the American Association for the Advancement of Science, 1997

Distinguished Professor of Chemistry, Wayne State University, 1997

Robert A. Welch Professor of Chemistry, Texas Tech University, 2004

Special Issue of the International Journal of Mass Spectrometry (Vol. 241, Nos. 2-3) was published to honor Bill Hase on his 60th birthday, 2005

Festschrift of the Journal of Physical Chemistry A (Vol. 110, No. 4, 2006) was published to honor Bill Hase's 60th birthday.

REPORT DOCUMENTATION PAGE

Form Approved
OMB No. 074-0188

1. AGENCY USE ONLY (Leave blank)	2. REPORT DATE	3. REPORT TYPE AND DATES COVERED
	3/31/06	Final Report, 8/1/02 - 12/31/05

4. TITLE AND SUBTITLE

Dynamics of O(3P) Reactions with Gaseous, Liquid, and Solid Hydrocarbons

5. FUNDING NUMBERS

FA9550-04-1-0373

6. AUTHOR(S)

William L. Hase

7. PERFORMING ORGANIZATION NAME(S) AND ADDRESS(ES)

Texas Tech University
Department of Chemistry and
Biochemistry
Lubbock, Texas 79409-1061

8. PERFORMING ORGANIZATION REPORT NUMBER

9. SPONSORING / MONITORING AGENCY NAME(S) AND ADDRESS(ES)

AFOSR
875 N Randolph St, Ste 325
Arlington VA 22203

10. SPONSORING / MONITORING AGENCY REPORT NUMBER

AFRL-SR-AR-TR-06-0127

11. SUPPLEMENTARY NOTES

12a. DISTRIBUTION / AVAILABILITY STATEMENT

Approve for Public Release: Distribution Unlimited

12b. DISTRIBUTION CODE

A

13. ABSTRACT ***(Maximum 200 Words)***

Prof. Hase has studied the reaction dynamics of oxygen atoms (triplet P state) with alkane hydrocarbons. In the initial phase, highly accurate ab initio quantum chemistry calculations (CASSCF, CASPT2, MRCI, with cc-pVTZ and cc-pVQZ basis sets) were applied to model reactions, including O + ethane and related reactions. In the second phase, a semiempirical quantum chemistry method, PM3-SRP, was developed by modifying and reparametrizing the standard PM3 method to fit the ab initio data. In the application phase, PM3-SRP was used in quasiclassical trajectory calculations to compute the dynamics of O + ethane at 5 eV collision energy, and propane monomer and tetramer at less than 2 eV collision energy. The trajectory results are in good agreement with experiment where comparison is possible. The O + ethane calculations at 5 eV predict the formation of a large number of products, many of which result from unimolecular decomposition of initially formed products. In the low energy O + propane calculations, the predicted distribution of vibrational and rotation energy in the OH product is in excellent agreement with experiment. In addition, energy transfer and physisorption of O atoms on self-assembled alkane monolayers were studied by computing inelastic scattering dynamics.

14. SUBJECT TERMS	15. NUMBER OF PAGES
	36
	16. PRICE CODE

17. SECURITY CLASSIFICATION OF REPORT	18. SECURITY CLASSIFICATION OF THIS PAGE	19. SECURITY CLASSIFICATION OF ABSTRACT	20. LIMITATION OF ABSTRACT